LETTER

doi:10.1038/nature10511

Aerobic bacterial pyrite oxidation and acid rock drainage during the Great Oxidation Event

Kurt O. Konhauser[1]*, Stefan V. Lalonde[1,2]*, Noah J. Planavsky[3], Ernesto Pecoits[1], Timothy W. Lyons[3], Stephen J. Mojzsis[4], Olivier J. Rouxel[2,5], Mark E. Barley[6], Carlos Rosière[7], Phillip W. Fralick[8], Lee R. Kump[9] & Andrey Bekker[10]

The enrichment of redox-sensitive trace metals in ancient marine sedimentary rocks has been used to determine the timing of the oxidation of the Earth's land surface[1,2]. Chromium (Cr) is among the emerging proxies for tracking the effects of atmospheric oxygenation on continental weathering; this is because its supply to the oceans is dominated by terrestrial processes that can be recorded in the Cr isotope composition of Precambrian iron formations[3]. However, the factors controlling past and present seawater Cr isotope composition are poorly understood. Here we provide an independent and complementary record of marine Cr supply, in the form of Cr concentrations and authigenic enrichment in iron-rich sedimentary rocks. Our data suggest that Cr was largely immobile on land until around 2.48 Gyr ago, but within the 160 Myr that followed—and synchronous with independent evidence for oxygenation associated with the Great Oxidation Event (see, for example, refs 4–6)—marked excursions in Cr content and Cr/Ti ratios indicate that Cr was solubilized at a scale unrivalled in history. As Cr isotope fractionations at that time were muted, Cr must have been mobilized predominantly in reduced, Cr(III), form. We demonstrate that only the oxidation of an abundant and previously stable crustal pyrite reservoir by aerobic-respiring, chemolithoautotrophic bacteria could have generated the degree of acidity required to solubilize Cr(III) from ultramafic source rocks and residual soils[7]. This profound shift in weathering regimes beginning at 2.48 Gyr ago constitutes the earliest known geochemical evidence for acidophilic aerobes and the resulting acid rock drainage, and accounts for independent evidence of an increased supply of dissolved sulphate[8] and sulphide-hosted trace elements to the oceans around that time[1,9]. Our model adds to amassing evidence that the Archaean-Palaeoproterozoic boundary was marked by a substantial shift in terrestrial geochemistry and biology.

Most contemporary seawater chromium is sourced from the dissolution of chromite [$(Fe,Mg)Cr(III)_2O_4$] in ultramafic rocks and soils[10]. Cr(VI) is a mobile phase under neutral to alkaline conditions, but the only naturally important oxidants of dissolved Cr(III) at pH < 9 are Mn(III)/Mn(IV)-oxides[11]. Instead, most solubilized Cr(III) is rapidly re-precipitated as $(Fe,Cr)(OH)_3$ at pH values >6, and so Cr tends to accumulate in modern soils as a Cr(III) residue[12]; at lower pH, soluble Cr(III) species dominate, even at high redox potential[7]. In modern oceans, the chromate (VI) anion, CrO_4^{2-}, is reduced to Cr(III) in the sediment via the action of Cr(VI)-reducing bacteria[13] and abiotically through reaction with Fe^{2+} or HS^- (ref. 14). During much of the Precambrian, similar reductive reactions would have occurred within the ocean water column, owing to the widespread development of ferruginous and/or euxinic conditions[15,16].

Given the efficient reduction of Cr(VI) and its subsequent quantitative removal as Cr(III), it was suggested that the isotopic composition of Cr in Precambrian sediments should reflect the magnitude of oxidative weathering of Cr(III) on land and the flux of Cr(VI) to the ancient oceans[3]. Motivated by this suggestion, we have compiled a database of Cr concentration in Precambrian iron formations (banded iron formations, BIFs, and granular iron formations, GIFs) and in Phanerozoic ironstones and hydrothermal precipitates (Fig. 1a; Supplementary Fig. 1; Supplementary Table 1). As Cr can be associated with detrital input because of its general insolubility, we evaluate authigenic Cr enrichment on the basis of Cr/Ti ratios normalized to evolving crustal values (Fig. 1b).

Our data show low Cr concentrations and a lack of large authigenic enrichment throughout much of the Archaean, although two exceptions exist. The first, a newly analysed sample from the 3.7–3.8-Gyr-old Isua BIF in Greenland with high Cr content, is likely to be related to Cr enrichment accompanying detrital chromite contamination. The second, a cluster of Algoma-type iron formations about 2.8–2.7 Gyr old, show high Cr concentrations and non-negligible authigenic Cr enrichment. These Algoma-type iron formations formed close to submarine volcanic arcs and spreading centres, and represent proximal exhalative deposits. Furthermore, some of them are associated with iron ore bodies indicative of significant post-depositional hydrothermal and oxidative alteration. Such caveats suggest that these Algoma-type iron formations cannot be used to infer Cr inputs from continental weathering.

By contrast, laterally extensive Superior-type iron formation deposits developed in near-shore shelf environments (see, for example, ref. 17) and are well suited to track continental Cr fluxes. Superior-type iron formations show minimal Cr concentrations and enrichments throughout the Archaean, but around 2.48 Gyr ago values become elevated in near-shore facies from the Penge and Kuruman formations (100–270 p.p.m. Cr, Cr/Ti enrichments up to 6× crustal values). The majority of deeper-water, clastic-material-free facies from the same iron formations show Cr concentrations <50 p.p.m. and Cr/Ti ratios within 3× of crustal values. Between 2.45 and 2.43 Gyr ago, the Weeli Wolli and the Cauê formations show more pronounced Cr concentrations and enrichments. Values then peak at 2.32 Gyr ago in the Timeball Hill Formation (>500 p.p.m. Cr and Cr/Ti ratios up to 10,000× crustal values).

Not all iron formations in this time window show elevated Cr concentrations or enrichments (for example, the Dales Gorge and Joffre members of the Brockman Iron Formation). Considering the low solubility of Cr(III) at marine pH (Supplementary Fig. 2), rapid reduction of Cr(VI), and near instantaneous co-precipitation of Cr(III) with ferric oxyhydroxide (Supplementary Fig. 3), Cr dispersal would be limited upon delivery to the oceans. In this regard, proximity of the depositional site to shore played a strong part in determining which iron formations would record a continental Cr input (Supplementary

[1]Department of Earth & Atmospheric Sciences, University of Alberta, Edmonton, Alberta T6G 2E3, Canada. [2]Université Européene de Bretagne, Institut Universitaire Européen de la Mer, Plouzané 29280, France. [3]Department of Earth Sciences, University of California, Riverside, California 92521, USA. [4]Department of Geological Sciences, University of Colorado at Boulder, Boulder, Colorado 80309, USA. [5]IFREMER, Centre de Brest, Plouzané 29280, France. [6]School of Earth and Environment, University of Western Australia, Crawley, Western Australia 6009, Australia. [7]Instituto de Geociências, Universidade Federal de Minas Gerais, Belo Horizonte, Minas Gerais 31270-91, Brazil. [8]Department of Geology, Lakehead University, Thunder Bay, Ontario P7B 5E1, Canada. [9]Department of Geosciences, The Pennsylvania State University, University Park, Pennsylvania 16827, USA. [10]Department of Geological Sciences, University of Manitoba, Winnipeg, Manitoba R3T 2N2 Canada.
*These authors contributed equally to this work.

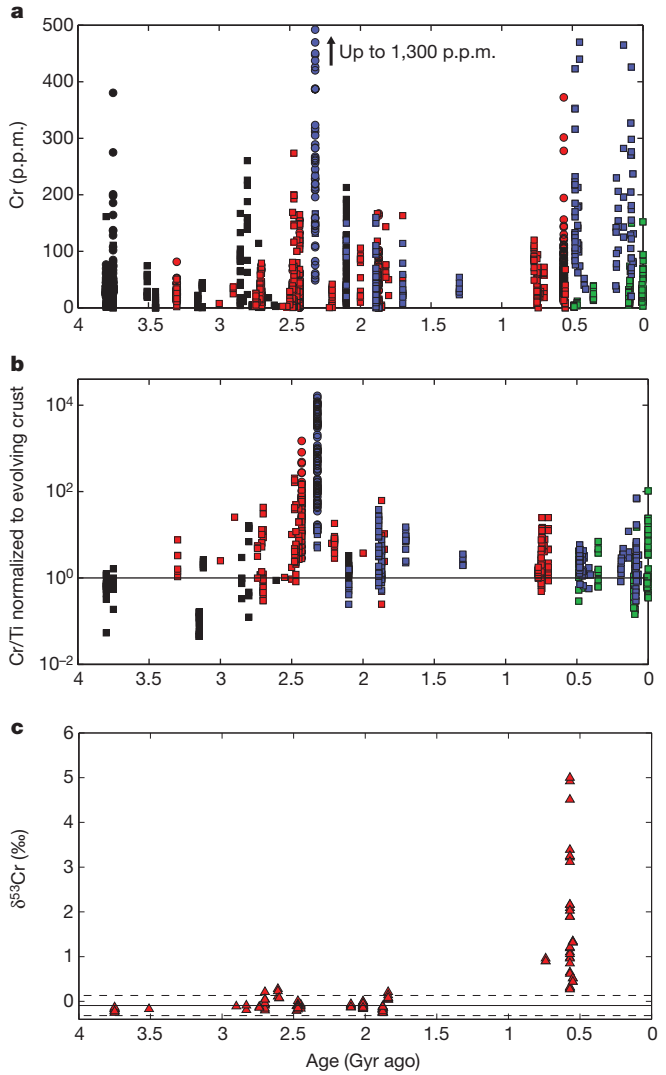

Figure 1 | Chromium in iron-rich sedimentary rocks through time. **a**–**c**, Presented are secular trends in Cr concentrations (**a**), authigenic enrichment in Cr relative to Ti (**b**), and Cr isotope values replotted from ref. 3 (**c**). In **a** and **b**, squares denote bulk analyses, circles are laser ablation analyses, black represents Algoma-type iron formations intimately related to submarine volcanism, red denotes Superior-type iron formations that formed in continental shelf environments, blue indicates Proterozoic oolitic iron formations and Phanerozoic ironstones that formed in shallow marine waters, and green represents Phanerozoic hydrothermal and exhalative deposits. Increased Cr concentrations and authigenic enrichments between 2.48 and 2.32 Gyr ago are related to increased Cr(III) inputs to sea water, and correspond to intense acidity generated by oxidative weathering of an untapped crustal pyrite reservoir. In **b**, Cr/Ti ratios have been normalized to the evolving Cr/Ti ratio of upper continental crust (solid line) according to the restoration model of ref. 32. In **c**, solid and dashed lines represent the mean and 2σ values, respectively, for Archaean and Palaeoproterozoic Cr isotope compositions from ref. 3. Significant positive Cr isotope fractionations in the Neoproterozoic indicate oxic Cr(VI) cycling and contrast with muted values in older iron formations representing a Cr cycle dominated by Cr(III).

Information section 1). Indeed, iron formations with some of the highest Cr values, such as the Cauê and Timeball Hill formations, show evidence of sediment re-working and grade into GIF and carbonate-facies, indicative of shallow-water deposition[18,19]. The oolitic Timeball Hill Formation (Supplementary Information section 2) records the highest degree of Cr enrichment in Palaeoproterozoic iron formations, which, according to our model, is not surprising considering its shallow water (pro-deltaic to offshore) deposition and unique position as a key formation in the chronology of the Great Oxidation Event (GOE)[4]. It is important to note that similarly shallow-water Superior-type iron formations from the Archaean—such as in the 3.25-Gyr-old Fig Tree Group, the 2.96-Gyr-old Pongola Supergroup and the 2.71–2.70-Gyr-old Beardmore-Geraldton Greenstone Belt—all have minimal enrichment, indicating limited continental supply of authigenic Cr before 2.48 Gyr ago.

After 2.32 Gyr ago, most iron-rich sedimentary rocks have high Cr concentrations but waning authigenic enrichments consistent with increasingly prevalent detrital contribution. These observations are confirmed by Cr-Ti-Al systematics, which show that Cr enrichments are highest between 2.48 and 2.32 Gyr ago and are maintained regardless of detrital input, whereas iron-rich sedimentary rocks younger than 2.32 Gyr ago typically have markedly higher Al_2O_3 content and Cr/Ti ratios approaching that of the average continental crust (Fig. 2). Time-binned means and 90th percentile values attest to the statistical significance of the observations outlined above (Supplementary Fig. 1c–f); considering all available data, the mean Cr/Ti ratio for the period 2.48–2.32 Gyr ago is more than an order of magnitude greater than that for any other period, significant to over 10 standard errors. Data averaged by source and unit, time-binned averages, and a schematic diagram summarizing different Cr inputs with time and changing iron formation depositional environments, are all given in the Supplementary Information (Supplementary Figs 1 and 4).

Authigenic Cr enrichments 2.48–2.32 Gyr ago indicate that a mechanism was in place that could supply Cr from insoluble chromite on land. On the basis of a small positive Cr isotope excursion ~2.7 Gyr ago, Frei *et al.*[3] argued for the initiation of an oxidative weathering cycle that included the reaction of O_2 with Mn(II) to form the MnO_2 catalyst required for Cr(III) oxidation and Cr(VI) supply to the oceans. However, the high partial pressure of O_2 required for Mn(II) oxidation at circumneutral pH (for example, ref. 20) strongly contradicts the preservation of sulphur isotope mass-independent fractionations (S-MIF) in the Archaean (for example, ref 21). Furthermore, the Archaean and Palaeoproterozoic iron formation Cr isotope values (0.28‰ to -0.26‰) fall almost entirely within two standard deviations about a mean of −0.09‰; this muted signal is in a strong contrast to Neoproterozoic values that reach up to +4.9‰ and are more indicative of oxic Cr mobilization (Fig. 1c). The ~2.7-Gyr-old iron formations that show positive Cr isotope values (for example, Boston, Temagami and Cherry Creek Metasupracrustal Suite) are Algoma-type, closely linked to submarine volcanism and hydrothermal activity.

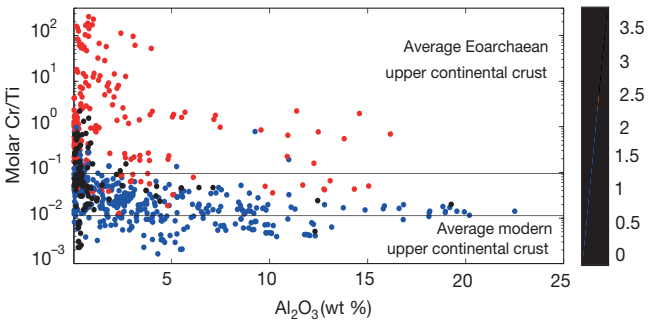

Figure 2 | Cr–Ti–Al systematics support the evolving nature of the marine Cr supply with time. In the Archaean (black circles), Algoma-type iron formations are closely linked to submarine volcanism and received limited clastic inputs (low Al_2O_3). In the period 2.5–2.3 Gyr ago (red circles), molar Cr/Ti ratios in iron formations significantly exceed crustal values, for both samples with high Al_2O_3 (for example, Timeball Hill Formation) and low Al_2O_3 (for example, Cauê Formation). We propose that this period represents unparalleled Cr solubilization on land and authigenic Cr supply to the oceans coincident with the onset of oxidative weathering. After 2.32 Gyr (blue circles), molar Cr/Ti ratios approach modern crustal values and indicate a stronger role for clastic Cr input. Oxidative mobilization of Cr(VI) in the Neoproterozoic and Phanerozoic are reflected only by mild Cr/Ti enrichments in samples with low Al_2O_3 contents.

Their rapid precipitation from fluids in disequilibrium may lead to amplification of small non-redox-dependent kinetic isotope effects, making such iron formations poorly suited to resolving atmospheric oxygenation. In addition, there are a number of difficulties with invoking an oxidized Mn intermediate and an increased supply of riverine Cr(VI) to sea water in the Archaean (see Supplementary Information section 3).

Although we agree that authigenic Cr enrichment in the early Palaeoproterozoic is linked to oxidative weathering, we propose an alternative model that does not require Cr(III) oxidation. It has been suggested that oxidative weathering of sulphide minerals (for example, pyrite) on land ~2.5 Gyr ago led to transiently increased delivery of chalcophilic trace elements and sulphate to the oceans[1,8]. Yet what has generally been overlooked is that these reactions also generate significant acidity. In the Archaean, increased atmospheric partial pressure of CO_2 may already have acidified surface waters to pH values around 4.7 (ref. 8), which would only be exacerbated by the acid generated by pyrite oxidation during the GOE[22]. That acid attack would have enhanced *in situ* dissolution of parent ultramafic/mafic material or Cr-bearing soil minerals that previously retained Cr under anoxic conditions, leading to increased marine Cr(III) supply: this increased supply could have been in dissolved form ($CrOH^{2+}$ or Cr^{3+}, depending on ambient pH), as Cr-enriched weathering products (for example, reactive clays and colloids), or perhaps, complexed with organic matter. Even today, Cr(III) can dominate riverine flux, and total riverine Cr flux increases with decreasing river pH (Supplementary Fig. 5). We suggest that the Cr enrichment beginning 2.48 Gyr ago reflects Earth's first acid rock drainage, where acidity was generated with rising O_2 at unprecedented scales through the oxidation of a previously untapped terrestrial pyrite reservoir. This process continued until the source of easily oxidizable pyrite diminished as the upper continental crust fully equilibrated with oxidized fluids.

In modern oxic soils, pyrite oxidation and the generation of acid rock drainage is only efficient with Fe(III) as the oxidant (see, for example, ref. 23). Accordingly, it is the ferrous iron to ferric iron oxidation reaction that is the rate-limiting step[24]; rate calculations show that in the absence of Fe(III) and at an atmospheric partial pressure of O_2 $<10^{-5}$ times the present atmospheric levels (Late Archaean estimate), inorganic pyrite oxidation is prohibitively slow, of the order of tens of thousands of years or greater for the dissolution of a 100 μm^3 pyrite cube (Supplementary Information section 4). Today, pyrite oxidation is dependent on aerobic respiration by chemolithoautotrophic bacteria capable of oxidizing Fe(II), as well as reduced sulphur, at O_2 concentrations <0.006 μM (ref 25). Thriving at low pH, they accelerate pyrite oxidation by several orders of magnitude and are wholly responsible for making pyrite oxidation self-propagating through concomitant production of dissolved Fe(III) as pH values drop below the threshold for inorganic Fe(II) oxidation (see, for example, ref. 26). Moreover, as very little energy is generated in the oxidation of ferrous to ferric iron, these bacteria must oxidize large amounts of Fe(II) in order to grow, and even a small number of cells can be responsible for generating significant acid rock drainage. Crucially, the acid that the bacteria produce drives weathering solutions to pH values below 4.5, at which point $(Fe,Cr)(OH)_3$ becomes increasingly soluble.

Cr(III) enrichments in iron formations may be used to constrain the pH of surface weathering solutions via a simple mixing model (Fig. 3). The model assumes that: (1) all Cr was sourced from a Cr-bearing weathering leachate mixed with river water, and precipitates quantitatively on mixing with seawater; and (2) all Fe was sourced from sea water. Assumption (1) is well supported by the strong pH dependence and rapid kinetics of Cr(III) precipitation (Supplementary Figs 2 and 3) and is conservative because we assume no loss of Cr during transport. Assumption (2) is also conservative, in that any Fe addition from river water only increases the required acidity for a given river/marine mixing ratio. The mixing model confirms that shallow deposits such as the Timeball Hill Formation should have been highly sensitive to the introduction of even small quantities of acidic, Cr-bearing continental fluids. As neither inorganic pyrite oxidation nor CO_2-driven weathering can produce levels of acidity below pH ~4.5 (see Supplementary Information section 4), Cr enrichment in iron formations 2.48–2.32 Gyr ago thus necessarily records acidic pyrite oxidation driven by the activity of aerobic Fe(II)-oxidizing bacteria, and constitutes strong evidence for their emergence on land by that time. This sequence of events agrees well with molecular studies suggesting that acidophilic chemolithoautotrophs diverged from the last common ancestor of α-, β- and γ-*Proteobacteria* around 2.5 Gyr ago[27].

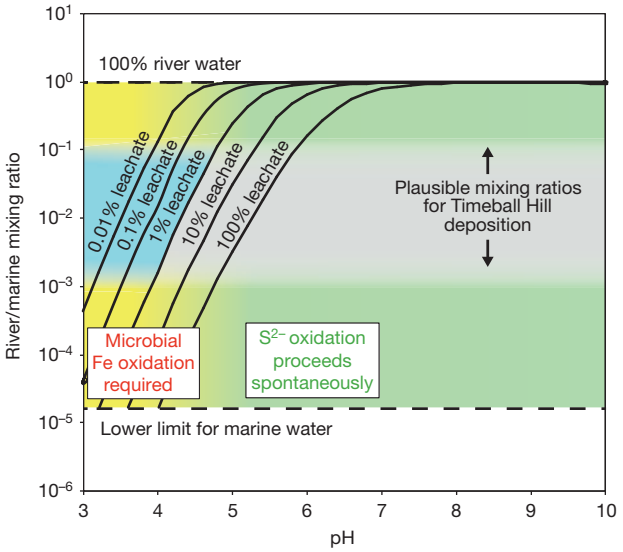

Figure 3 | River/marine mixing model, indicating alteration pH necessary to supply sufficient Cr to account for Cr enrichment in the Timeball Hill Formation. The model is conservatively based on the lower end of Cr enrichment reported for the Timeball Hill Formation, specifically mean Cr (197 p.p.m.) and Fe (47 wt%) values[29]. Black lines, mixing trajectories for Fe-bearing marine waters contributing a total of 10 p.p.m. Fe, and river water bearing different proportions of Cr leachate, in which Cr concentration is limited as a function of pH by amorphous $Cr(OH)_3$ solubility according to Supplementary Fig. 2a. Light blue shaded area, plausible leachate contributions and mixing ratios that are realistic for the deposition of Timeball Hill Formation (Supplementary Information section 1.5). The green to yellow transition indicates the dependence of inorganic pyrite oxidation on pH, and the approximate pH threshold below which aerobic microbial Fe(II) oxidation is required to sustain pyrite oxidation. The mixing model confirms that aerobic microbial Fe(II) oxidation was required to account for the low alteration pH and Cr mobilization even for Timeball Hill Formation samples with the lowest degrees of Cr enrichment: our own measured Cr values are higher and thus push the lines to more acidic values. Lower limit for marine water was estimated by considering the reservoir size of continental runoff relative to the modern marine reservoir (data from ref. 33).

Apart from our Cr record in iron formations, independent geochemical constraints support a change in continental weathering by the early Palaeoproterozoic. For instance, despite similar parent lithologies, the 2.7-Gyr Mt Roe palaeosol has a Cr concentration more than five times greater than the 2.45-Gyr-old Denison palaeosol (Supplementary Table 2); the former also has higher and more homogenous Cr/Ti ratios, indicating a more conservative Cr behaviour. Both are characterized by Fe loss: the older example reflecting formation under an anoxic atmosphere[28], and the younger, by our model, pointing to acidity associated with pyrite oxidation that would have prevented Fe(III) precipitation even if some oxygen was present. Additional evidence for intensification of chemical weathering on land is given by elevated values of the chemical index of alteration (CIA) and high Al/Ti ratios in early Palaeoproterozoic shales (Supplementary Information section 5). Indeed, the shales of the Timeball Hill Formation,

which shows the highest Cr enrichments in this study, have CIA values ranging from 97.9 to 99.7 (ref. 29).

The Cr isotope record in iron formations (ref. 3) provides key evidence for our proposed model of Cr(III) transport during the GOE. Cr(III) oxidation in the Archaean and early Palaeoproterozoic, if a factor, was unlikely to have been quantitative because of the still low partial pressure of O_2 and high O_2 demand for Mn(II) oxidation. As a result, large Cr isotope fractionations (of the order of the maximum theoretical fractionation associated with Cr(III) oxidation, up to 7‰; ref. 30) would be expected in the dissolved pool if it was dominated by oxidized Cr(VI). However, minimal Cr isotope fractionation in iron formations during that time, despite pronounced Cr enrichments, requires transport of an isotopically unfractionated Cr load, which could only be igneous-rock-derived Cr(III). Iron formations in the Neoproterozoic provide a strong contrast to those in the Archaean and Palaeoproterozoic. Values of δ^{53}Cr in the ~715-Myr-old Rapitan Formation and the ~700-Myr-old Chuos Formation exceed Archaean and Palaeoproterozoic δ^{53}Cr values by a factor of three; by 560 Myr ago, the Yerbal Formation has δ^{53}Cr values more than 15 times higher, approaching 5‰, as expected for a Cr(VI)-dominated marine supply[3]. The most parsimonious explanation for the discrepancy in Cr systematics between Palaeoproterozoic and Neoproterozoic iron formations is a shift from O_2 levels sufficient for the oxidation of some highly redox-sensitive elements (such as S and Fe) and a marine Cr supply dominated by Cr(III), to more oxidizing conditions permitting widespread Mn(II) and Cr(III) oxidation, accompanied by an increased role for Cr(VI). Authigenic Cr enrichments in the Neoproterozoic and Phanerozoic remain well below those observed at ~2.48–2.32 Gyr ago, despite oxic Cr(VI) input; we emphasize that the Palaeoproterozoic Cr excursion should be unique because of the 'switch' from anoxic to oxic regimes of terrestrial pyrite weathering.

The present work has important implications for the timing, duration and sequence of events associated with the GOE. It reveals the GOE as a protracted process, first expressed in the early signs of oxidative weathering manifested in our Cr record, as well as other proxies[1,8,9], and culminating at 2.32 Gyr ago with the permanent loss of the S-MIF signal[4]. The evolution and activity of microbes is intimately linked with the redox evolution of the Earth's surface, but as demonstrated here, sometimes in unexpected ways. Redox-sensitive elemental proxies for the rise of atmospheric oxygen need to be considered in the light of a wide gamut of possible biogeochemical influences beyond simple oxidation because, paradoxically, it is Cr cycling in the reduced form that tracks the onset of oxidative weathering. Intriguingly, the ability of cyanobacteria in the ocean's photic zones to influence their own nutrient supply via O_2-enhanced chemical weathering may represent an unrecognized positive biological feedback. Moreover, unlike carbonic-acid-driven weathering, the increased delivery of phosphate from sulphuric acid weathering of apatite would be unaccompanied by increased alkalinity. This decoupling of nutrient and alkalinity fluxes would drive a proportional increase in organic carbon burial, a necessary condition for the generation of positive carbon isotope excursions (see, for example, ref. 31). The ~2.25–2.10-Gyr Lomagundi carbon isotope excursion may, together with the Cr enrichment documented here, be a manifestation of sulphuric acid driven weathering produced during the initial sedimentary cycle of oxidative weathering[22].

METHODS SUMMARY

Cr, Ti and Al concentrations, representing more than 100 Precambrian iron formations and Phanerozoic ironstone/hydrothermal samples and consisting of 2,021 separate data points, were amassed from previously published bulk analyses and from new analyses on both bulk and grain-by-grain (haematite and magnetite only) scales. Samples selected for new geochemical analyses include both drill core and hand samples from fresh exposures. Oxidized surfaces, veins and strongly recrystallized zones were avoided to minimize the effects of weathering and diagenetic or metamorphic overprinting. New analyses were performed at the University of Alberta using a Perkin Elmer Elan6000 quadrupole ICP-MS (inductively-coupled plasma-mass spectrometer) on powdered sample digests in solution mode and *in situ* on epoxy mounts using a New Wave UP-213 laser ablation system. At the Woods Hole Oceanographic Institution, powdered samples were analysed in solution mode using a ThermoElectron Element2 high-resolution ICP-MS. Instrument calibration was achieved using commercial standard solutions and verified against international glass standards NIST 610 and 612 at the University of Alberta and geostandards IF-G and BHVO-1 at the Woods Hole Oceanographic Institution. Cr isotope data presented by Frei *et al.*[3] are replotted in Fig. 1c and reported in δ notation relative to NIST SRM 979.

Full Methods and any associated references are available in the online version of the paper at www.nature.com/nature.

Received 10 March 2010; accepted 26 August 2011.

1. Anbar, A. D. *et al.* A whiff of oxygen before the Great Oxidation Event? *Science* **317,** 1903–1906 (2007).
2. Wille, M. *et al.* Evidence for a gradual rise of oxygen between 2.6 and 2.5 Ga from Mo isotope and Re-PGE signatures in shale. *Geochim. Cosmochim. Acta* **71,** 2417–2435 (2007).
3. Frei, R., Gaucher, C., Poulton, S. W. & Canfield, D. E. Fluctuations in Precambrian atmospheric oxygenation recorded by chromium isotopes. *Nature* **461,** 250–253 (2009).
4. Bekker, A. *et al.* Dating the rise of atmospheric oxygen. *Nature* **427,** 117–120 (2004).
5. Papineau, D., Mojzsis, S. J. & Schmitt, A. K. Multiple sulfur isotopes from Paleoproterozoic Huronian interglacial sediments and the rise of atmospheric oxygen. *Earth Planet. Sci. Lett.* **255,** 188–212 (2007).
6. Guo, Q. *et al.* Reconstructing Earth's surface oxidation across the Archean-Proterozoic transition. *Geology* **37,** 399–402 (2009).
7. Rai, D., Eary, L. E. & Zachara, J. M. Environmental chemistry of chromium. *Sci. Total Environ.* **86,** 15–23 (1989).
8. Reinhard, C. T. *et al.* A Late Archean sulfidic sea stimulated by early oxidative weathering of the continents. *Science* **326,** 713–716 (2009).
9. Scott, C. *et al.* Tracing the stepwise oxygenation of the Proterozoic ocean. *Nature* **452,** 456–459 (2008).
10. Shiraki, K. Geochemical behaviour of chromium. *Resour. Geol* **47,** 319–330 (1997).
11. Oze, C., Bird, D. K. & Fendorf, S. Genesis of hexavalent chromium from natural sources in soil and groundwater. *Proc. Natl Acad. Sci. USA* **104,** 6544–6549 (2007).
12. Oze, C. *et al.* Chromium geochemistry of serpentine soils. *Int. Geol. Rev.* **46,** 97–126 (2004).
13. Wang, P.-C. *et al.* Isolation and characterization of an *Enterobacter cloacae* strain that reduces hexavalent chromium under anaerobic conditions. *Appl. Environ. Microbiol.* **55,** 1665–1669 (1989).
14. Fendorf, S. E. Surface reactions of chromium in soils and waters. *Geoderma* **67,** 55–71 (1995).
15. Holland, H. D. The oxygenation of the atmosphere and oceans. *Phil. Trans. R. Soc. B* **361,** 903–915 (2006).
16. Lyons, T. W., Reinhard, C. T. & Scott, C. Redox redux. *Geobiology* **7,** 489–494 (2009).
17. Bekker, A. *et al.* Iron formation: the sedimentary product of a complex interplay among mantle, tectonic, oceanic, and biospheric processes. *Econ. Geol.* **105,** 467–508 (2010).
18. Spier, C. A., de Oliveira, S. M. B., Sial, A. N. & Rios, F. J. Geochemistry and genesis of the banded iron formations of the Cauê Formation, Quadrilátero Ferrífero, Minas Gerais, Brazil. *Precambr. Res.* **152,** 170–206 (2007).
19. Eriksson, K. A. The Timeball Hill Formation: a fossil delta. *J. Sedim. Res.* **43,** 1046–1053 (1973).
20. Morgan, J. J. Kinetics of reaction between O_2 and Mn(II) species in aqueous solutions. *Geochim. Cosmochim. Acta* **69,** 35–48 (2005).
21. Pavlov, A. A. & Kasting, J. F. Mass-independent fractionation of sulfur isotopes in Archean sediments: strong evidence for an anoxic Archean atmosphere. *Astrobiology* **2,** 27–41 (2002).
22. Holland, H. D. Volcanic gases, black smokers, and the Great Oxidation Event. *Geochim. Cosmochim. Acta* **66,** 3811–3826 (2002).
23. Moses, C. O. *et al.* Aqueous pyrite oxidation by dissolved oxygen and by ferric iron. *Geochim. Cosmochim. Acta* **51,** 1561–1571 (1987).
24. Singer, P. C. & Stumm, W. Acidic mine drainage: the rate-determining step. *Science* **167,** 1121–1123 (1970).
25. Gleisner, M., Herbert, R. B. Jr & Frogner Kockum, P. C. Pyrite oxidation by *Acidithiobacillus ferrooxidans* at various concentrations of dissolved oxygen. *Chem. Geol.* **225,** 16–29 (2006).
26. Nordstrom, D. K. & Southam, G. in *Geomicrobiology: Interactions Between Microbes and Minerals* (eds Banfield, J. F. & Nealson, K. H.) 361–390 (Vol. 35, Mineralogical Society of America, 1997).
27. Blank, C. E. Evolutionary timings of the origin of mesophilic sulphate reduction and oxygenic photosynthesis: a phylogenomic dating approach. *Geobiology* **2,** 1–20 (2004).
28. Rye, R. & Holland, H. D. Paleosols and the evolution of atmospheric oxygen: a critical review. *Am. J. Sci.* **298,** 621–672 (1998).
29. Dorland, H. C. *Paleoproterozoic Laterites, Red Beds and Ironstones of the Pretoria Group with Reference to the History of Atmospheric Oxygen.* M.Sc. thesis, Rand Afrikaans Univ., (1999).

30. Schauble, E., Rossman, G. R. & Taylor, H. P. Theoretical estimates of equilibrium chromium-isotope fractionations. *Chem. Geol.* **205,** 99–114 (2004).
31. Aharon, P. Redox stratification and anoxia of the early Precambrian oceans: implications for carbon isotope excursions and oxidation events. *Precambr. Res.* **137,** 207–222 (2005).
32. Condie, K. C. Chemical composition and evolution of the upper continental crust: contrasting results from surface samples and shales. *Chem. Geol.* **104,** 1–37 (1993).
33. Berner, E. K. & Berner, R. A. *Global Environment: Water, Air, and Geochemical Cycles* (Prentice Hall, 1996).

Supplementary Information is linked to the online version of the paper at www.nature.com/nature.

Acknowledgements This study was supported by the Natural Sciences and Engineering Research Council of Canada (K.O.K., S.V.L., A.B., P.W.F.), the National Science Foundation Division of Earth Sciences (T.W.L., O.J.R., L.R.K.), the National Science Foundation's Graduate Research Program (N.J.P.), the Agouron Institute (E.P., T.W.L.), NASA's Exobiology Program (T.W.L., S.J.M.), NASA's Astrobiology Institute (T.W.L., L.R.K., N.J.P.), the Australian Research Council (M.E.B.), and the Conselho Nacional de Desenvolvimento Cientifico e Technológico (C.R.) We also thank V. Suckau (USIMINAS) for sample collection, G. Chen for assistance with LA-ICP-MS analyses, and J. Robbins for data compilation.

Author Contributions Samples were provided by K.O.K., N.J.P., E.P., S.J.M., O.J.R., M.E.B., C.R., P.W.F. and A.B.; K.O.K. conceived the study; E.P. and N.J.P. performed the geochemical analyses; and S.L. conducted the data reduction and statistical analyses. K.O.K., S.V.L. and N.J.P. produced the manuscript with significant contributions from all co-authors. Specifically, insights into the geological setting for a number of samples were provided by E.P., M.E.B., C.R., P.W.F. and A.B.; use of geochemical proxies to assess Palaeoproterozoic weathering and seawater composition by T.W.L., O.J.R., L.R.K. and A.B.; and the timing and duration of the GOE by S.J.M., L.R.K. and A.B.

Author Information Reprints and permissions information is available at www.nature.com/reprints. The authors declare no competing financial interests. Readers are welcome to comment on the online version of this article at www.nature.com/nature. Correspondence and requests for materials should be addressed to K.O.K (kurtk@ualberta.ca).

METHODS

Sample selection. In our previous work[34], the interpretation of trace element signatures in iron formations as proxies of ancient sea water warranted a pre-selection of samples with minimal detrital influence based on chemical composition. One method commonly used to differentiate detritally-sourced components versus authigenic precipitation is through measurement of incompatible elements, such as Al, Ti, Zr, Th, Hf and Sc[35]. However, both the low solubility of Cr(III) and the rapid reduction of Cr(IV) in the presence of Fe(II) makes it highly unlikely that Cr in iron formations is representative of bulk ocean water. Instead, the focus of this study was to ascertain Cr fluxes from land to the marginal marine setting, and in this regard, shallow water iron formations (as well as their Phanerozoic counterparts, ironstones) are valuable proxies even if they include a significant detrital component. Thus, we present here all available iron formation and ironstone data. Only bulk-digest analyses of potential iron ores (possessing >50 wt% Fe, an upper boundary for iron formations[36]) or iron oxide-rich rocks that are believed to have formed through metasomatic processes (for example, iron oxide copper-gold ore deposits) have been excluded. Also, it is important to note that in our compilation of 2,021 data points sample preparation and analytical techniques varied; in order to avoid selective bias to our results, all available data were included.

Cr analyses of iron formations. Data are presented in Supplementary Table 1. Iron formation and ironstone samples selected for new geochemical analyses include both drill core and hand samples from fresh exposures. Oxidized surfaces, veins and strongly recrystallized zones were avoided to minimize the effects of weathering and diagenetic or metamorphic overprinting. At the University of Alberta, samples for bulk major and trace element analysis were cut in slabs, broken into small chips (<5 mm) without metal contact, and powdered in an automated agate mill. Crushed rock powders (<100 mesh) were dissolved with heated HF+HNO_3 and analysed using a Perkin Elmer Elan6000 Quad-ICP-MS (quadrupole inductively coupled plasma mass spectrometer). Accuracy and precision of the analytical protocol were verified with the use of well-established international whole rock standards (for example, BE-N Basalt, CRPG Nancy; see http://research.eas.ualberta.ca/rif/quad_icp_ms.html). *In situ* trace element analyses were performed on polished epoxy mounts using the same Quad-ICP-MS connected to a laser ablation system operating with spot sizes of 20 to 60 μm. Optimisation of ICP-MS parameters (RF power 1,200 W, peak hopping acquisition, 50 ms dwell time) were achieved by ablating either the NIST SRM 610 (~400 p.p.m. Cr) or NIST SRM 612 (~40 p.p.m. Cr) international glass standards. For quantitative trace element determinations, the NIST 610 and 612 standards and iron formation/ironstone samples were ablated using identical conditions with spot sizes of either 20 μm or 60 μm, 5 Hz repetition rate and energy density of ~13 J cm^{-2}. Quantitative results were obtained via the calibration of relative element sensitivities against the NIST 610 and 612 standards. Data reduction and calculations of concentrations were done using the GLITTER (XP version, New Wave Research) laser ablation software. Repeated analysis ($n = 10$) of the NIST 612 using a 60 μm spot size yielded relative standard deviations of between 5 and 15% (2σ level) and a detection limit of 3 p.p.m. for Cr.

At the Woods Hole Oceanographic Institution, clean samples of iron formations were crushed between two Plexiglas discs inside a polypropylene bag using a hydraulic press. Rock chips were rinsed several times with deionized water during ultrasonication. The cleaned material was powdered in an agate shatterbox. Iron formation and ironstone sample powders were weighed in 5 ml Teflon beakers and dissolved using 2 ml of concentrated trace-metal grade HNO_3 with 2 ml of concentrated HF. After evaporation on a hot plate at 50 °C, complete dissolution and Fe oxidation were achieved by a second evaporation step using 4 ml of *aqua regia*. The dry residue was then dissolved in 4 ml of 6 N HCl and 1 drop of H_2O_2 by heating at 40 °C in a closed vessel. Organic carbon was not attacked by this procedure and was always present in trace amounts. Trace and major element analysis were performed on a ThermoElectron Inc. Element2 ICP-MS. Samples were spiked with 5 p.p.b. of internal In standard to correct for changes in instrument sensitivity during the analytical session. Unknown sample concentrations were calibrated against matrix-matched, multi-elemental standards prepared with Specpure plasma solution standards. Based on multiple analyses of randomly selected samples across multiple analytical sessions, accuracy for Cr was >95%. Analytical precision and accuracy were also checked by multiple analyses of the geostandards IF-G and BHVO-1.

Cr isotope data presented by Frei *et al.*[3] are replotted in Fig. 1c and reported in δ notation relative to NIST SRM 979. For Cr isotope analytical details and additional information regarding available data and samples, see Frei *et al.*[3].

River/marine mixing model. The mixing model was constructed using thermodynamic constraints on Cr(III) solubility and approximate calculations that make several simple assumptions as to the source and fate of Cr and Fe upon mixing of river and marine waters in a shallow, marginal marine setting. These assumptions include: (1) that all Cr is sourced from a soil leachate solution in which Cr concentration is governed by equilibrium with amorphous $Cr(OH)_3$; (2) that in order to account for surface runoff and areas of pyrite-free catchment, the soil leachate solution constitutes some fraction (that is, 0.01 to 100% leachate contours in Fig. 3) of the total riverine input; (3) that all Fe is sourced from sea water containing 10 p.p.m. Fe; and (4) that any given iron formation Cr/Fe ratio represents a constraint that the model must respect through appropriate mixing of river and marine inputs and quantitative precipitation of both Cr and Fe. Data representing the lower end of mean Cr/Fe values reported for the Timeball Hill iron formation (197 p.p.m. Cr, 47 wt% Fe, molar Cr/Fe of 0.00046; ref. 29) was chosen as a conservative model target in terms of iron formation Cr/Fe ratio; data from this study indicate significantly higher values and even more acidic conditions during the deposition of the Timeball Hill iron formation.

Cr(III) solubility as a function of pH was calculated for a solution saturated with respect to amorphous $Cr(OH)_3$, at 25 °C and in 0.01 M NaCl to mimic freshwater conditions, using the equilibrium modelling suite Visual Minteq version 2.61 (ref. 37) with the default supplied database thermo_minteq.dat (Supplementary Fig. 2). For each pH examined in the mixing model, the question becomes what river/marine mixing ratio is required, for a given leachate/river mixture, to supply Cr and Fe in the correct proportion to satisfy the iron formation Cr/Fe constraint, based on 10 p.p.m. Fe in sea water and Cr(III) in river water derived from pH-dependent solubility data. This approach can be considered conservative by the employment of the lower end of Cr/Ti enrichments for the Timeball Hill iron formation and by the fact that any Fe brought in by river water, any marine Fe concentrations above 10 p.p.m., and any Cr lost during transport all serve to increase the required mixing ratio and thus indicate greater acidity.

34. Konhauser, K. O. *et al.* Oceanic nickel depletion and a methanogen famine before the Great Oxidation Event. *Nature* **458,** 750–753 (2009).
35. Chester, R. *Marine Geochemistry* (Blackwell, 2000).
36. Klein, C. Some Precambrian banded iron-formations (BIFs) from around the world: their age, geologic setting, mineralogy, metamorphism, geochemistry, and origin. *Am. Mineral.* **90,** 1473–1499 (2005).
37. Gustafsson, J. P. Visual Minteq. http://www.lwr.kth.se/English/OurSoftware/vminteq/ (verified, 23 August 2011).